Double-slit experiment with single wave-driven particles and its relation to quantum mechanics

Anders Andersen,[1,*] Jacob Madsen,[1] Christian Reichelt,[1] Sonja Rosenlund Ahl,[1]
Benny Lautrup,[2] Clive Ellegaard,[3] Mogens T. Levinsen,[3] and Tomas Bohr[1,†]

[1]*Department of Physics and Center for Fluid Dynamics, Technical University of Denmark, DK-2800 Kgs. Lyngby, Denmark*
[2]*Niels Bohr International Academy, The Niels Bohr Institute, Blegdamsvej 17, DK-2100 Copenhagen Ø, Denmark*
[3]*The Niels Bohr Institute, University of Copenhagen, Blegdamsvej 17, DK-2100 Copenhagen Ø, Denmark*

(Received 13 October 2014; published 6 July 2015)

In a thought-provoking paper, Couder and Fort [Phys. Rev. Lett. **97**, 154101 (2006)] describe a version of the famous double-slit experiment performed with droplets bouncing on a vertically vibrated fluid surface. In the experiment, an interference pattern in the single-particle statistics is found even though it is possible to determine unambiguously which slit the walking droplet passes. Here we argue, however, that the single-particle statistics in such an experiment will be fundamentally different from the single-particle statistics of quantum mechanics. Quantum mechanical interference takes place between different classical paths with precise amplitude and phase relations. In the double-slit experiment with walking droplets, these relations are lost since one of the paths is singled out by the droplet. To support our conclusions, we have carried out our own double-slit experiment, and our results, in particular the long and variable slit passage times of the droplets, cast strong doubt on the feasibility of the interference claimed by Couder and Fort. To understand theoretically the limitations of wave-driven particle systems as analogs to quantum mechanics, we introduce a Schrödinger equation with a source term originating from a localized particle that generates a wave while being simultaneously guided by it. We show that the ensuing particle-wave dynamics can capture some characteristics of quantum mechanics such as orbital quantization. However, the particle-wave dynamics can not reproduce quantum mechanics in general, and we show that the single-particle statistics for our model in a double-slit experiment with an additional splitter plate differs qualitatively from that of quantum mechanics.

DOI: 10.1103/PhysRevE.92.013006 PACS number(s): 47.55.D−, 03.65.−w, 05.45.−a

I. INTRODUCTION

In a beautiful series of investigations initiated by Couder and Fort it has been shown that many phenomena, earlier believed to belong exclusively to the realm of quantum mechanics, are actually observable in a system as indisputably classical as a millimeter sized droplet of silicone oil bouncing on a vertically vibrating bath of the same liquid. Standing waves can form on the liquid surface due to the vibrations as first noted by Faraday in 1831. Faraday waves appear when the amplitude of vibration is above a threshold, which depends on the viscosity and the depth of the liquid layer [1,2]. At a vibration amplitude just below the onset of the Faraday wave instability, the droplets can, strangely enough, spontaneously break the symmetry and start moving horizontally over the surface, being pushed along by the waves they generate [3–6].

Couder and Fort immediately noticed the similarity of the walking droplets (walkers) with de Broglie's picture of quantum particles guided by their "pilot waves" [7]. It was subsequently demonstrated that the system can actually reproduce quantumlike effects such as orbital quantization [8–13] and tunneling through a barrier [14]. It has further been shown that the probability distribution generated by letting a droplet explore the surface of a small container over an extended period of time can look like the solution of a wave equation [15]. The group of Couder and Fort also pioneered the theoretical modeling of the coupled droplet-wave dynamics [6,8]. Building upon these first models, Bush and co-workers systematically developed a hydrodynamical pilot-wave theory which successfully captures the droplet dynamics and the wave generation far from boundaries and subsurface barriers [11,16–19]. For an overview of both experiments and theories, see the review by Bush [20].

The walkers in fact seem close to the so-called "double solution theory" proposed by de Broglie [21]. This theory introduces a "real" wave field localized near a "real" particle, being simultaneously excited by the particle and guiding it. Using such a deterministic system of interacting waves and particles, the theory thereby attempts to underpin the statistical framework of quantum mechanics and the statistical Schrödinger wave. The work on walking droplets has thus led to a renewed interest in "realistic" quantum mechanics in the spirit of Einstein and de Broglie [20,22,23].

The problem that gets closest to the heart of quantum mechanics is the double-slit experiment with walking droplets investigated by Couder and Fort in 2006 [7]. In the double-slit experiment, one is not studying stationary states where a droplet explores an extended region of space for a long period of time, but states where a droplet traverses the system only once, possibly interfering with its own wave on its way through the double-slit arrangement. It is thus a very direct probe of the superposition of paths, which is so central in quantum mechanics.

In this paper, we shall study the double-slit experiment, both from an experimental and a theoretical point of view. First, we question the main conclusion drawn by Couder and Fort in their double-slit experiment with walking droplets [7]. We then present the results of our own double-slit experiment. To shed light on the interference mechanism in the double-slit experiment, we present individual trajectories and wave fields during droplet passage through the double-slit arrangement. We also

*Corresponding author: aanders@fysik.dtu.dk
†tbohr@fysik.dtu.dk

discuss the challenges that we believe remain to be resolved to obtain reproducible single-particle statistics and to draw firm conclusions from observed interference patterns in this type of experiments. Second, we review the standard quantum mechanical description of the double-slit experiment in terms of the time evolution of a wave packet, and we compare this to a modified version of the experiment with a central splitter plate and find that the splitter plate does not significantly influence the interference pattern. Third, we present a deterministic particle-wave dynamics in the spirit of the ideas proposed by de Broglie [21]. We shall argue that it is not possible in general to capture quantum mechanical results in such a model system, where the trajectory of the particle is well defined. In particular, we show that the superposition of paths embodied in the quantum mechanical double-slit experiment with a central splitter plate can not be reproduced in the particle-wave model system when the splitter plate is sufficiently long.

II. DOUBLE-SLIT EXPERIMENT WITH WALKING DROPLETS

A. Double-slit experiment by Couder and Fort

Couder and Fort concluded in their double-slit experiment with walking droplets that an interference pattern in the single-particle statistics is produced by interference between the waves passing the two slits and that the interference pattern is well fitted by a Fraunhofer diffraction and interference expression [7]. We question this conclusion for the following reasons: In the experiment, only 75 droplet passages of the slits are recorded ([7], Fig. 3). This small number is increased by left-right symmetrization, which, however, does not improve the statistics, and the experimental data are only presented in the symmetrized form. To submit the data to a χ^2 test we have used the maximum likelihood estimator $\chi^2 = 2\sum_{i=1}^{N} O_i \ln(O_i/E_i)$, where O_i is the observed number of trajectories falling in the ith bin and E_i the expected number. Using the χ^2 test, a fit to a Gaussian distribution is found to be just as good as the fit to the Fraunhofer interference pattern presented in the paper. In addition, the single-slit result (blue envelope curve) is not backed up by data because the single-slit results in the paper are for slits of different widths ([7], Fig. 2). Finally, the single-particle statistics in the single-slit and the double-slit experiment are compared with the absolute value of the amplitude in the Fraunhofer diffraction and interference expressions for the corresponding geometries. These expressions are not derived theoretically for the droplets and it is not motivated why the absolute value of the amplitude rather than the absolute square is the relevant quantity for comparison.

B. Experimental setup

In our experiments with walkers we used three different aluminum cells: a reference cell without a subsurface barrier, a cell with a single slit, and a cell with a double-slit geometry (Fig. 1). We have chosen a wedge-shaped opening in all cells to best represent a well-defined droplet source. The subsurface barriers were 5.0 mm thick horizontally and 3.5 mm in height above the level of the flat bottom. The slits were 5.0 mm wide and the distance between the slit centers in the double-slit experiment was 10.0 mm. The filling depth of the cells was 4.1 mm, so that the shallow liquid layer above the barriers was 0.6 mm deep. Each cell was milled out of a single piece of aluminum and connected firmly by an aluminum cone to the table of a Brüel and Kjær 4809 vibration exciter. The resulting motion was monitored using a Brüel and Kjær 4367 single-axis accelerometer mounted on the table of the vibration exciter. Our experimental cells were constructed so that the resonance frequencies of the cone plus cell structure were all above 1 kHz. We did not characterize the possible variation of the vertical acceleration over the experimental cells and the possible horizontal acceleration. Both quantities should ideally be monitored in experiments on walking droplets as discussed by Harris and Bush [24].

We used a silicone oil with viscosity 20 Pa s. The cells were forced vertically with simple harmonic motion with frequency 80 Hz and amplitude $\gamma = 3.9g$, where g is the acceleration due to gravity. In the deep layer the theoretical Faraday wavelength was 4.75 mm and the measured Faraday threshold

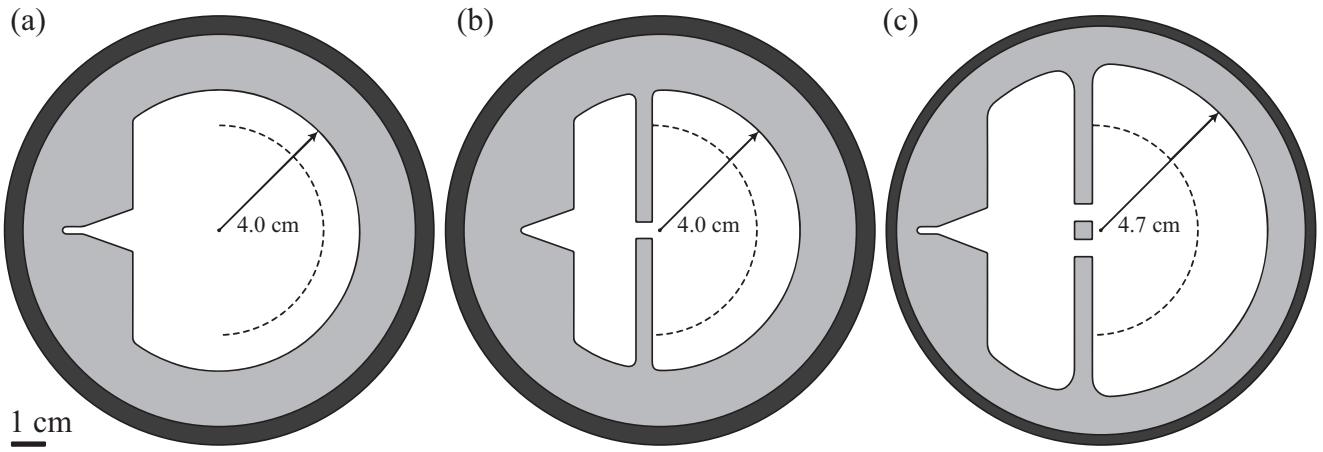

FIG. 1. Schematic illustrations of the experimental cell geometries seen from above. (a) Reference experiment with no barrier, (b) single slit, and (c) double slit. The outer rim (dark) encloses the shallow layer (light gray) and the deep layer (white) where the Faraday waves can be excited and the walkers move. The droplet trajectory deflection angles were determined from the points at which the droplets crossed the dashed circle segments with radius 3.0 cm.

amplitude was $\gamma_F = 4.1g$. Therefore, the dimensionless distance to the Faraday threshold $\Gamma = (\gamma_F - \gamma)/\gamma_F$ took the value $\Gamma = 0.049$ in our experiment, and the corresponding value of the memory parameter was $\Gamma^{-1} = 21$.

To monitor possible air currents above the experimental cells we suspended a 10 mm × 10 mm piece of paper with thickness 80 μm using a 25 cm long thread with diameter 20 μm. Even weak ambient air currents led to easily observable motion of the suspended paper, and by shielding the experimental cells using a Perspex cylinder we were able to significantly reduce but not completely eliminate air currents above the cells.

The droplet diameter was determined using a digital SLR camera equipped with a macro lens. In all experiments, we used selected silicone oil droplets with diameter 0.75 ± 0.03 mm. We illuminated the experimental cells from above using a small halogen lamp, a diffuser screen, and a large 50:50 optical beam-splitter that was placed at an angle of 45° above the cells. The droplets were video recorded with a digital SLR camera pointing vertically down on the cells, and the droplets were identified and tracked using custom written software.

C. Trajectories and single-particle statistics

In the double-slit experiment each droplet was guided into the wedge-shaped opening by hand using a long pointed rod. Subsequently, the rod was removed to release the droplet [Fig. 2(a)]. The opening directed the droplet towards the double-slit arrangement [Fig. 2(b)]. Approximately 20% of the released droplets passed the double-slit barrier at first impact [Fig. 2(c)], and after passage the droplets typically moved at some angle relative to the line of symmetry [Fig. 2(d)]. The reference experiment without a barrier and the single-slit experiment were carried out with similar procedures.

The measured droplet trajectories in the reference experiment and the trajectories of the droplets that at first impact passed the slit arrangements in the two different slit experiments show important characteristics.

From the reference experiment we only show trajectories of the droplets that would have passed through a virtual single slit with geometry similar to our single-slit arrangement, i.e., in the range -0.3 cm $< y < 0.3$ cm at $x = -0.5$ cm in accordance with the distribution of the droplet impact parameter at the slit entrance. The droplets in the reference experiment move out of the wedge-shaped opening directed on average along the line of symmetry [Fig. 3(a)]. Once the droplets have left the wedge-shaped region they typically follow straight trajectories until they approach the outer boundary on the opposite side of the cell. Eventually, the

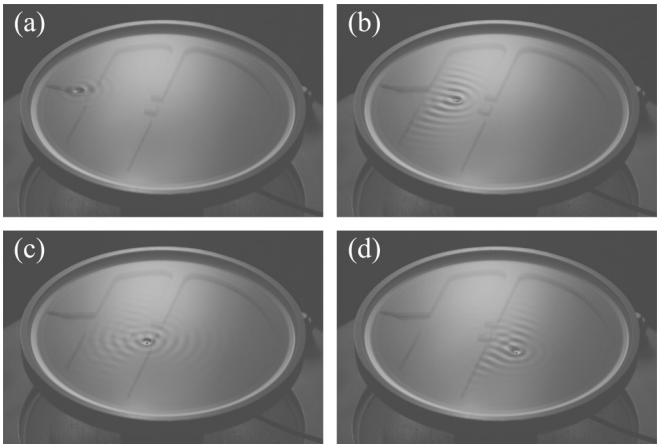

FIG. 2. Snapshots of a walker in the double-slit experiment. (a), (b) The droplet is propelled by the pilot wave towards the subsurface barrier with two slits. (c) The droplet follows a well-defined trajectory through one of the slits, whereas the pilot wave is free to pass through both slits. (d) After passage, the droplet moves along a deflected path.

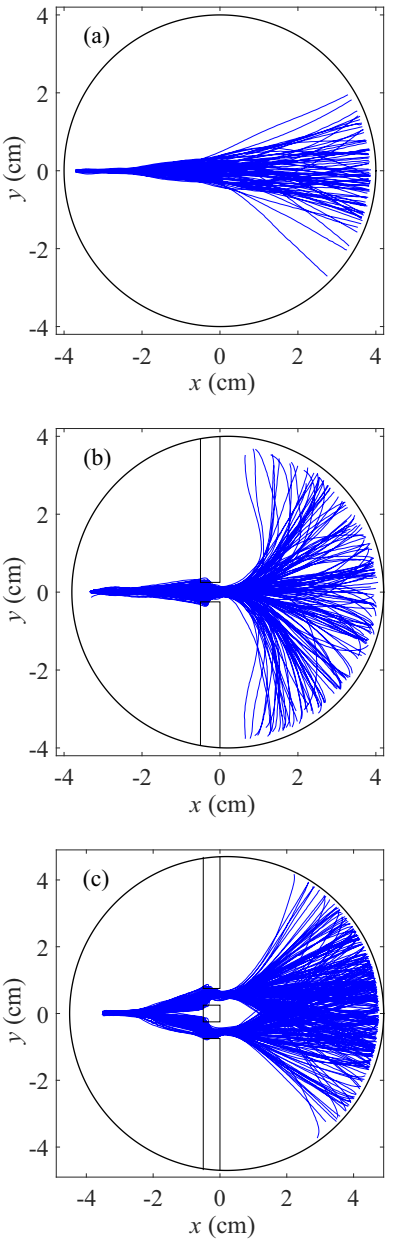

FIG. 3. (Color online) Droplet trajectories. (a) Reference experiment without a barrier, 78 trajectories, (b) single-slit experiment, 169 trajectories, and (c) double-slit experiment, 301 trajectories. In (a) we only show the trajectories of the droplets that would have passed through a virtual single slit with geometry similar to our single-slit arrangement, and in (b) and (c) we only show the trajectories of the droplets that passed the slit arrangement at first impact.

droplets are either reflected or caught in circular trajectories along the boundary.

In the single-slit experiment, the interaction with the slit boundary leads to a trajectory envelope with a characteristic constriction at the exit of the slit [Fig. 3(b)]. Similar trajectory envelopes are found for each of the two slits in the double-slit experiment with the important difference that the trajectory envelope behind the slit arrangement is more narrow than in the single-slit experiment [Fig. 3(c)]. In both the single- and the double-slit experiments, most of the droplet impacts are not perpendicular to the barrier in contrast to the droplet impacts in the experiment by Couder and Fort [7]. Also, the distributions of the droplet impact parameter are not uniform over the slit openings in both the single- and the double-slit experiments (Fig. 4). In particular, we note that our choice of a centrally located droplet source results in many droplet impacts near the central barrier that separates the two slits in the double-slit experiment and few impacts in the outer halves of the two slits.

From each droplet trajectory we extracted the deflection angles α and made histograms based on the number of counts N (Fig. 5). Error bars $\pm\sqrt{N}$ are shown as uncertainty estimates. The deflection angle of a droplet was determined as the angle between the line of symmetry and the line from the origin of our system of reference to the point where the droplet

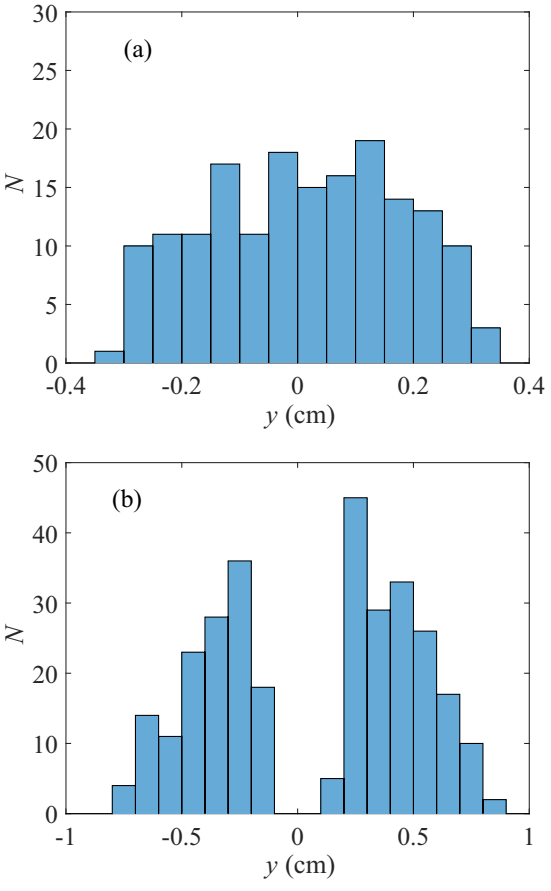

FIG. 4. (Color online) Histograms with the number of counts N showing the distributions of the droplet impact parameter y at the slit entrances at $x = -0.5$ cm. (a) Single-slit experiment, 169 trajectories and (b) double-slit experiment, 301 trajectories.

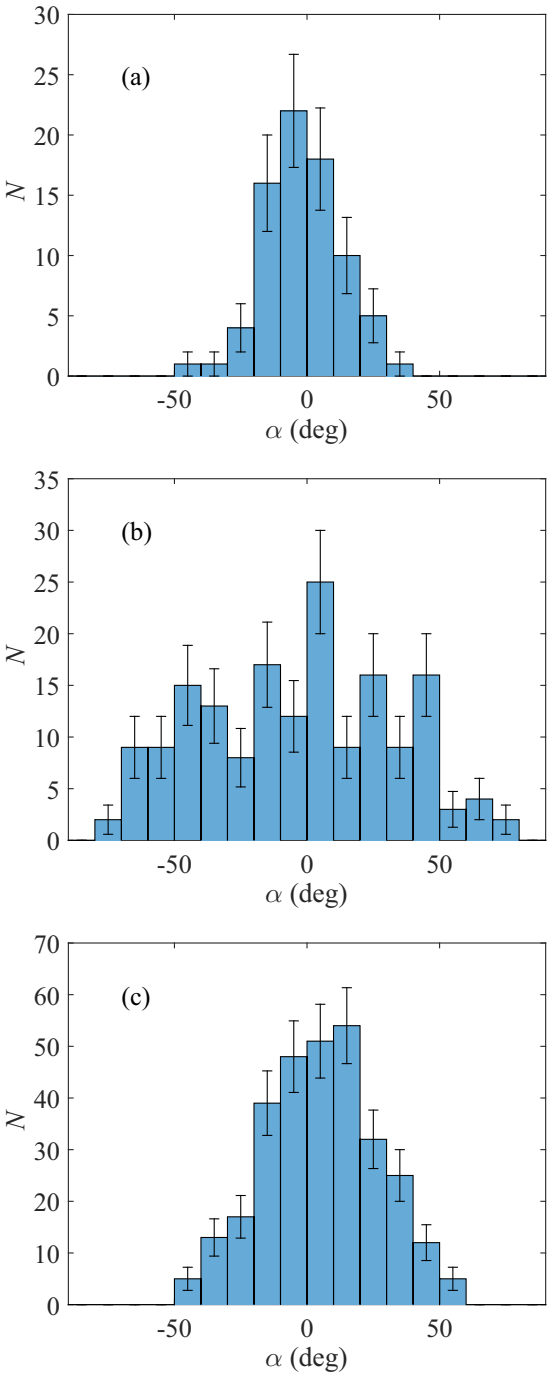

FIG. 5. (Color online) Histograms with the number of counts N showing the single-particle statistics based on the deflection angles α. (a) Reference experiment without a barrier, 78 trajectories, (b) single-slit experiment, 169 trajectories, and (c) double-slit experiment, 301 trajectories.

trajectory crossed a circle with radius 3.0 cm centered at the origin (Fig. 1). This procedure is different from the method applied by Couder and Fort who determined the deflection angle of a droplet from the orientation of the final straight part of the trajectory [7]. We prefer our procedure since it does not rely on the assumption of straight droplet trajectories far from boundaries and the necessity to disregard the influence of the

outer cell boundary on the droplet dynamics, something which at least in our cells would not be possible. The histograms show small left-right asymmetries that are presumably due to imperfections in alignment, but which also partly reflects the rather small number of trajectories. We therefore only present our original histograms and we do not left-right symmetrize our data as done by Couder and Fort [7]. We see that the presence of the single slit significantly broadens the distribution of deflection angles in comparison with the reference experiment. The double-slit distribution is more narrow than the single-slit distribution most likely due to the differences in the distribution of impact positions and angles of the droplets. Most notably, we do not see any clear interference pattern in the two slit experiments.

D. Slit passage, correlations, and wave fields

The walkers can be influenced strongly by the corners and the sides of the subsurface barrier during passage of the slits in the double-slit experiment [Fig. 6(a)]. The droplets slow down from the walking speed 1.5 cm s^{-1} that in our experiment is characteristic of a freely walking droplet far from external boundaries and subsurface barriers to a speed that can be as low as 0.6 cm s^{-1} [Fig. 6(b)]. In some realizations, the speed reduction leads to a doubling of the passage time in comparison with the passage time 0.33 s that a droplet moving with the walking speed 1.5 cm s^{-1} perpendicularly through the double-slit arrangement would have. To estimate the time scale τ for the decay of the Faraday waves, we consider the memory parameter and use the expression $\tau/T_F \approx \Gamma^{-1}$, where T_F is the period of the Faraday waves [25]. With $T_F = 0.025$ s and $\Gamma^{-1} = 21$ we find that $\tau \approx 0.53$ s. The time scale for the decay of the Faraday waves and the typical droplet passage time are therefore comparable. The droplets that experience the most significant speed reduction typically move near and even over the corners of the boundaries of the double-slit configuration. The detailed slit boundary geometry could therefore significantly influence droplet trajectories and passage times, and it must be accounted for carefully in experimental studies.

To explore the possible connection between droplet impact and trajectory after slit passage we show the deflection angle as function of the impact parameter a few centimeters before the slits and at the entrance to the slits (Fig. 7). In the first case, we do not see a correlation, but in the second situation there is a clear correlation between the impact parameter and the deflection angle. This result appears to contrast the study

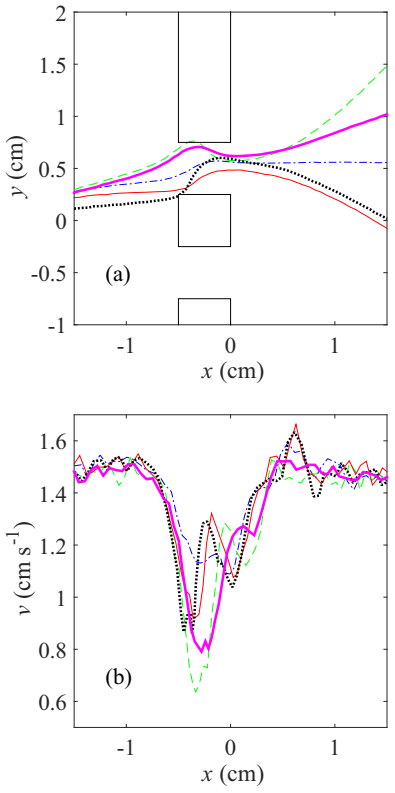

FIG. 6. (Color online) Trajectories and droplet speeds in the double-slit experiment. (a) Five selected trajectories during passage of the slit and (b) the corresponding droplet speeds. The slit passage times of the droplets from $x = -0.5$ to 0.0 cm were 0.46 s (dotted-dashed line, blue), 0.67 s (dashed line, green), 0.50 s (solid line, red), 0.63 s (dotted line, black), and 0.58 s (thick solid line, magenta).

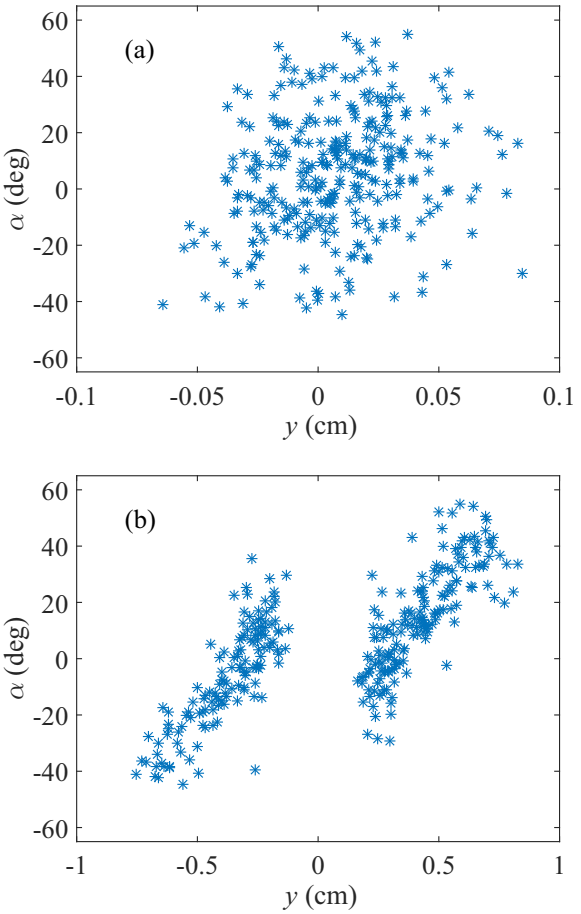

FIG. 7. (Color online) Correlation between droplet impact parameter y and trajectory deflection angle α after slit passage in the double-slit experiment with 301 trajectories. (a) Droplet impact parameter before the double slit at $x = -3.0$ cm and (b) at the entrance to the slits at $x = -0.5$ cm.

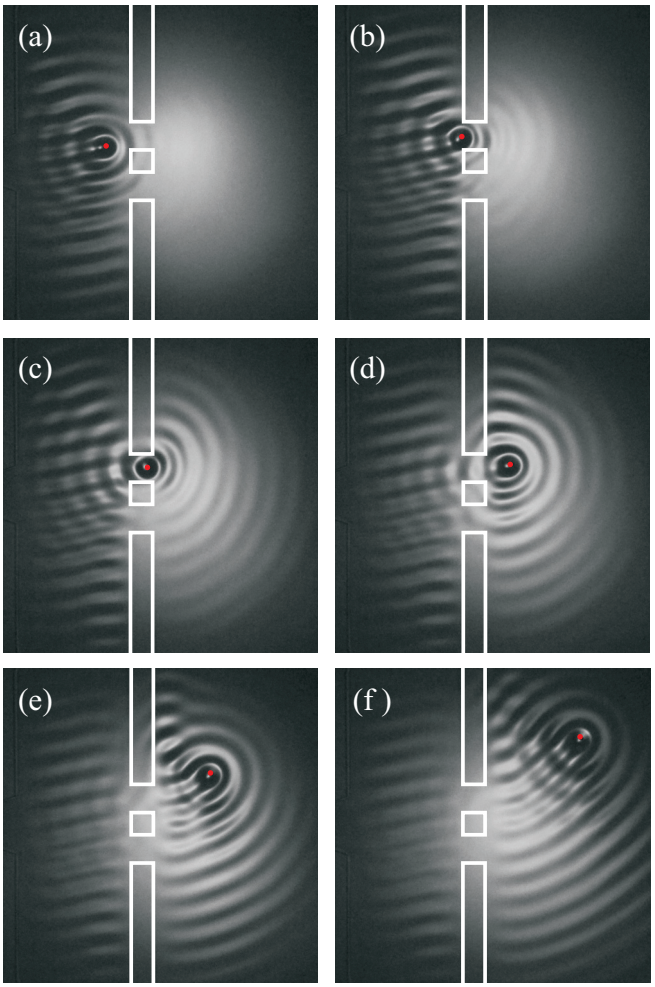

FIG. 8. (Color online) Time series of a walking droplet and the associated wave in the double-slit experiment. The red dot highlights the position of the droplet, and the double slit is accentuated in white.

by Couder and Fort, in which they conclude that there is no correlation between impact parameter and deflection angle [7].

We now turn from the droplet motion to the wave fields of the walkers in the double-slit configuration (Fig. 8). We find that the wave field behind the double-slit arrangement appears to be weak in (a) and (b) when the droplet is entering the slit opening. Also, it seems that it is difficult to excite the wave field in the other slit opening and the component of the wave field that passes the other slit appears to be insignificant. We note that when the droplet is at the entrance to the double-slit arrangement in (b), the wave crests behind the chosen slit appear as circle segments with a slowly varying intensity. If the wave contribution through the other slit were significant, we would expect the wave intensity of these wave crests to be modulated on a length scale comparable to the Faraday wavelength. The strength of the wave field behind the double-slit arrangement dramatically increases when the droplet exits the slit in (c). After passage of the slit, there is a large amplitude behind the double-slit arrangement as shown in (d)–(f), but there is still no discernible modulation of the wave crests. We presume that these qualitative features of the wave field will be generic provided that the slit width is smaller than or comparable to the Faraday wavelength.

III. QUANTUM MECHANICAL DOUBLE-SLIT EXPERIMENT

To discuss the possibilities of wave-driven particle systems as analogs to quantum mechanics, we first present as reference a numerical simulation of the standard quantum mechanical version of the double-slit experiment, and a new modified version with a central longitudinal splitter plate placed before the two slits.

The numerical simulations are performed using two-dimensional nonrelativistic quantum mechanics discretized on a lattice, and set in a finite box, such that the wave function vanishes on the boundary. We followed a wave packet by representing the time evolution operator in Cayley's form to ensure unitarity, and solving the discrete Schrödinger equation with the alternating direction implicit method (see [26], pp. 1049 and 1052).

We start off with the Gaussian wave packet

$$\psi(x,y) = A\exp[ik_x x - (x/\alpha_x)^2 - (y/\alpha_y)^2], \qquad (1)$$

where A is the amplitude, k_x the wave number, and α_x and α_y the width parameters. The wave packet carries an initial momentum only in the direction towards the double slit. We shall measure all dimensions in units of the associated wavelength $\lambda = 2\pi/k_x$ that equals six grid units on our square computational grid.

The wave packet, with $\alpha_x = 1.67$ and $\alpha_y = 8.33$, is first placed in a potential equivalent to the standard double-slit experiment, i.e., it is placed in a finite box of dimensions 50×50 with two slits separated by a barrier of length 5.00. Both the barrier width and the two slit openings measure 1.67. The wave packet moves towards the double slit where part of it is reflected by the barrier, whereas the rest is transmitted through the slits and creates an interference pattern (Fig. 9). An identical wave packet in the alternate version of the double-slit experiment undergoes diffraction as it impinges on the central splitter plate of length 12.50 introduced before the double slit, and a small part of the wave is also reflected. The diffracted parts continue towards the double slit where the two parts go through the two slits and create an interference pattern (Fig. 10).

In both simulations, the two parts of the wave packet arrive at the two different slits exactly in phase and give rise to the same kind of interference pattern (Fig. 11). The transmitted probability density will in general differ in the two scenarios due to the difference in reflections, but the accumulated probability density at a fixed distance behind the slits exhibit the same minima and maxima (Fig. 12). The transmitted probability for the chosen parameters is in fact greatest in the case with a central splitter plate because the diffraction guides a larger fraction of the wave packet through the two slits. As expected, we have found that the splitter plate does not change the interference structure observed after the double-slit arrangement in quantum mechanics.

As mentioned above, we use Dirichlet conditions on all boundaries. Such boundary conditions generate reflected waves (Fig. 11). However, within the time interval of the

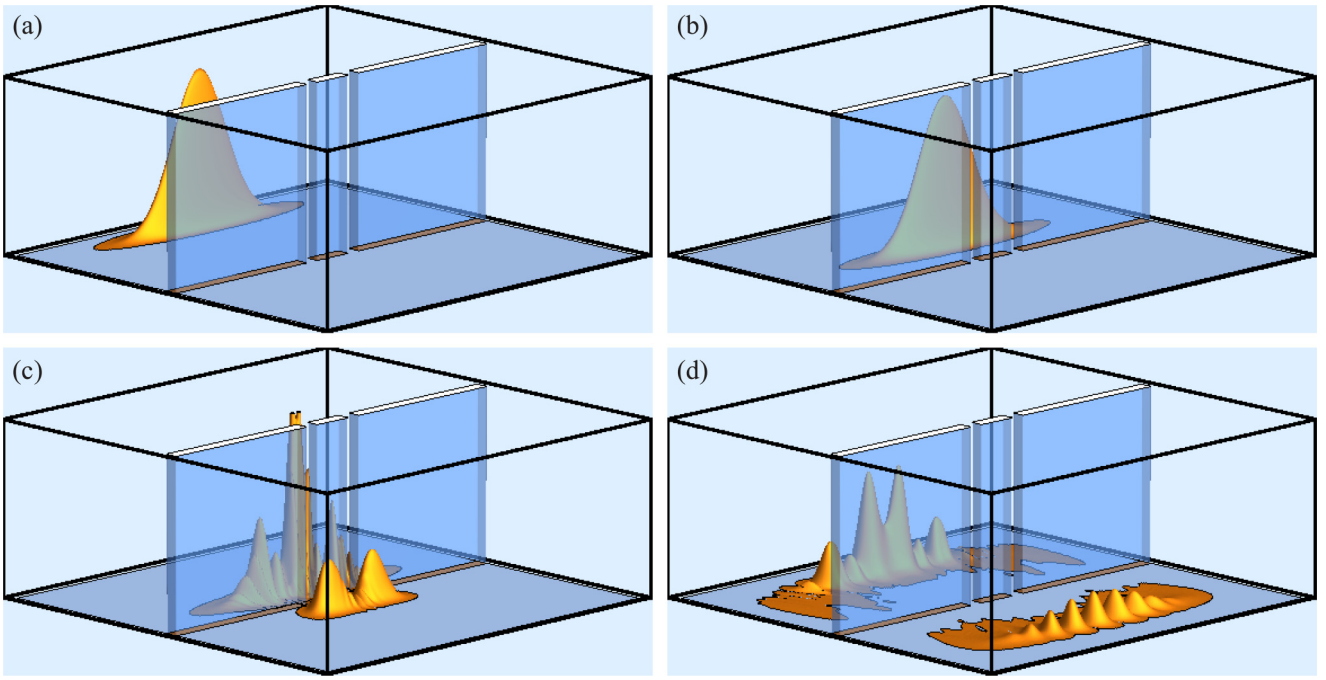

FIG. 9. (Color online) Time evolution of the probability density of a wave packet in the standard quantum mechanical double-slit experiment.

simulations, the only reflections seen are due to the barrier and the splitter plate. Indeed, the sampling leading to the accumulated probability density (Fig. 12) has been made within a time interval where no appreciable reflections have occurred due to the downstream boundaries. This was ensured by selecting a wave packet, which is sufficiently narrow in the x direction, a domain which is sufficiently broad, and a location of the sampling "screen" sufficiently far from the end wall of the box. If the simulations were continued for a very long time, the multiple reflections from the boundaries would in the end dominate the picture and tend to wash out the interference pattern that we are interested in.

IV. SIMPLE THEORY FOR WAVE-DRIVEN PARTICLES AS ANALOGY TO QUANTUM MECHANICS

The theoretical description of the walking droplets in the literature has so far been concentrated on developing

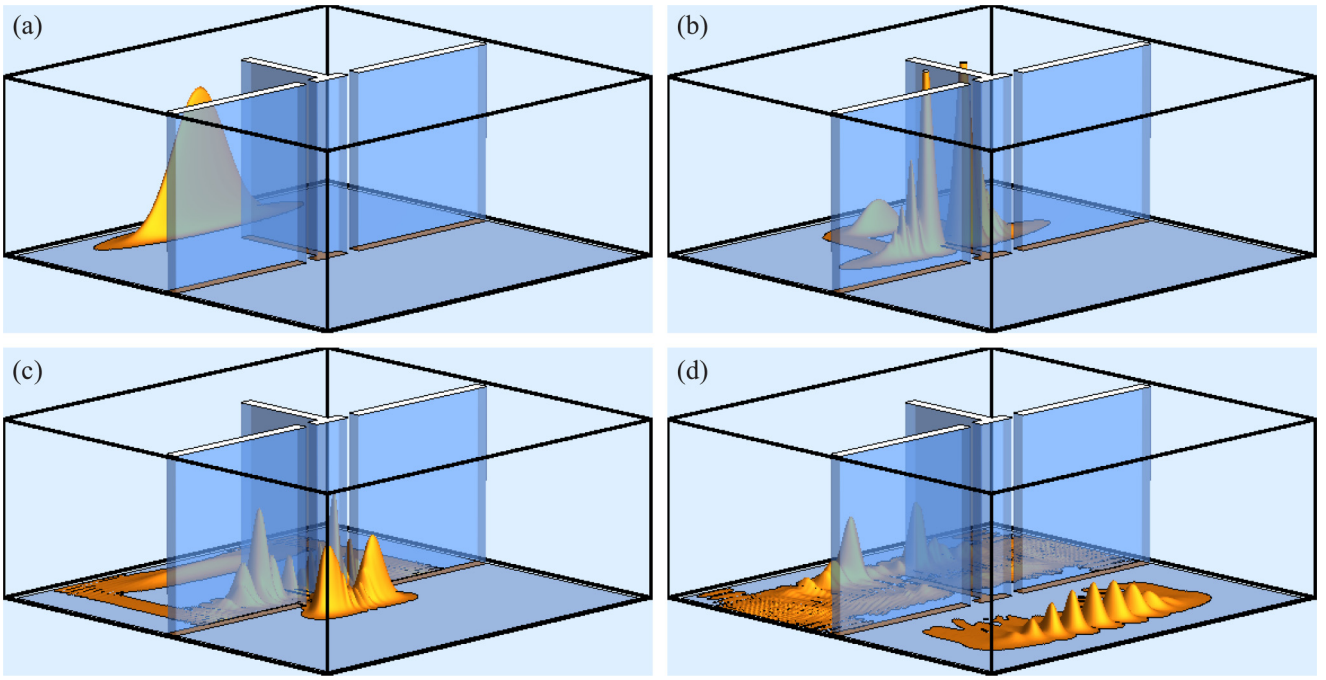

FIG. 10. (Color online) Time evolution of the probability density of a wave packet in the quantum mechanical double-slit experiment with a central splitter plate.

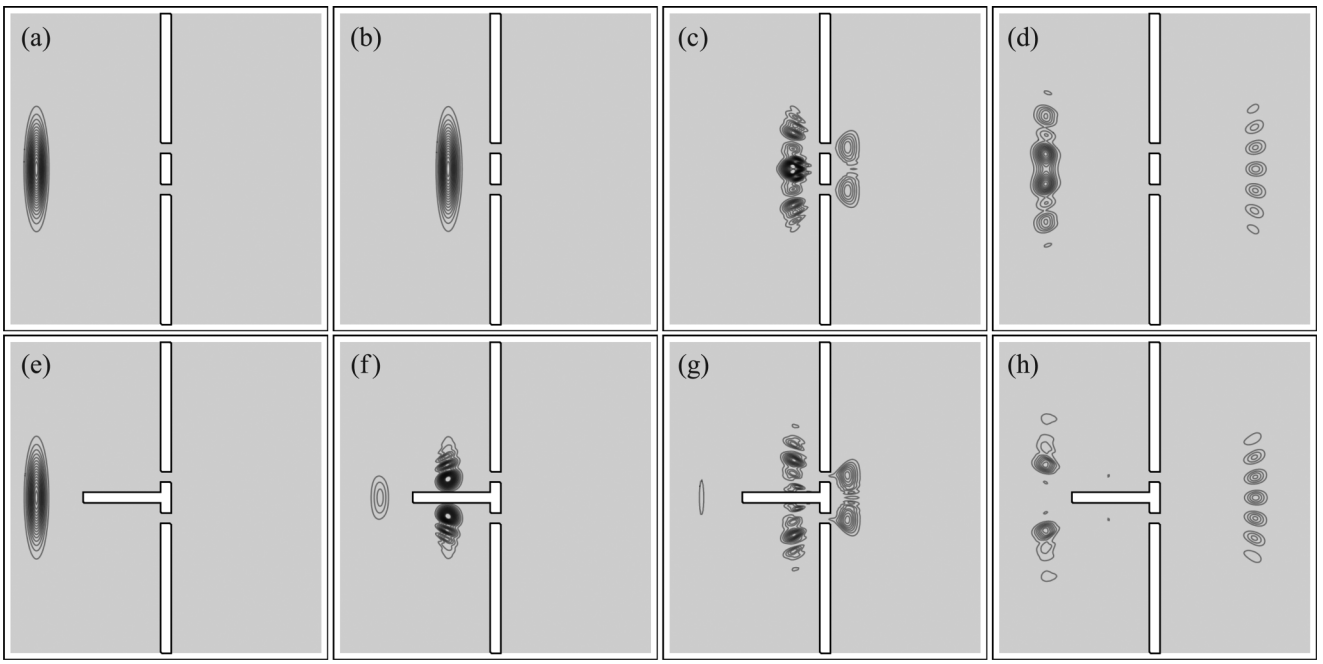

FIG. 11. Time evolution of a quantum mechanical wave packet, showing the contours of the probability density as it goes through a double slit without a central splitter plate (a)–(d), and with a splitter plate (e)–(h).

a hydrodynamical pilot-wave theory, where both the wave excitations created by the bouncing droplets and the thrust and drag on the droplets supplied by those waves have been modeled [16–19]. In this way, one can compute the path of a walker far away from boundaries or barriers and, e.g., verify the "Landau levels" found when mounting the system on a rotating table [8–11]. However, it seems very difficult from such an approach to understand the connection between the droplet dynamics and quantum mechanics. In this work, we shall take a very different, more abstract, approach, where we do not attempt to give an accurate description of the hydrodynamics of the walking droplets. Instead, we shall consider a simple but generic particle-wave dynamics based on the Schrödinger equation and ideas by de Broglie. Our aim will be to explore possibilities and limitations of our model that we surmise are common to particle-wave models in general.

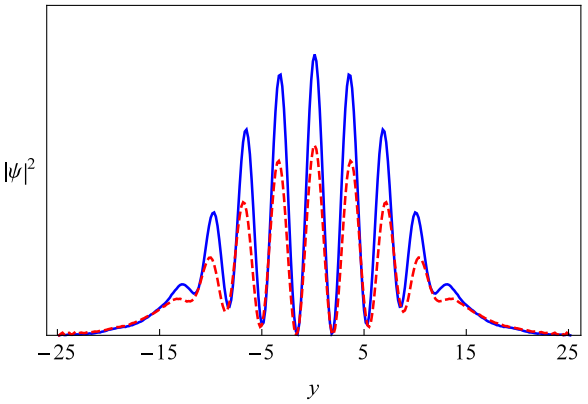

FIG. 12. (Color online) Accumulated probability density at the cross section at 15.83 after the slit arrangement in the standard quantum mechanical double-slit experiment (dashed line, red) and with a central splitter plate (solid line, blue). The slit openings were 1.67 wide, the width of the central barrier was 5.00, and the length of the central splitter plate was 12.50.

A. A framework for particle-wave dynamics

In the work of de Broglie a theoretical picture is presented, which is surprisingly close to the experiments on walkers. In his double solution theory, de Broglie proposes that, aside from the Schrödinger wave function, which only has statistical significance and thus is normalized, there might be a "real" wave, which acts like a guiding wave for a "real" particle, while the particle is responsible for exciting the wave [21]. This picture is very different from Bohm's interpretation of quantum mechanics, where one solves the Schrödinger equation for the problem at hand and then lets the particle move in that field without influencing it [27–29]. In de Broglie's picture, the Schrödinger equation only emerges as a probability density for the particles, but there is another underlying wave field, closely associated with the particle, a wave field which so far has not been observed.

A simple way of implementing this type of particle-wave dynamics in a nonrelativistic setting is to take the standard Schrödinger equation and add an inhomogeneous source term $J(\mathbf{r},t)$ stemming from a particle at a given position $\mathbf{r}_p(t)$. Thus, we write

$$\left(i\hbar\frac{\partial}{\partial t}-\hat{H}\right)\Psi(\mathbf{r},t)=J(\mathbf{r},t), \tag{2}$$

where the complex wave field $\Psi(\mathbf{r},t)$ can be expressed in terms of two real functions of space and time, an amplitude a and a phase Φ:

$$\Psi(\mathbf{r},t)=a(\mathbf{r},t)e^{i\Phi(\mathbf{r},t)}. \tag{3}$$

The homogeneous equation would thus have dispersive plane-wave solutions respecting de Broglie's relation $\lambda = h/p$ relating wavelength and velocity (momentum) of particles in quantum mechanics. In the following we shall show that the (suitably) forced equation will have localized wave solutions excited by the particle and simultaneously moving it. The simplest possibility for the source term is to take the inhomogeneity to be located exactly at the position of the particle

$$J(\mathbf{r},t) = A(t)\delta[\mathbf{r} - \mathbf{r}_p(t)]. \tag{4}$$

This equation has to be supplemented by an equation of motion for the particle, and there the natural choice is the guidance equation

$$\mathbf{v}_p(t) \equiv \dot{\mathbf{r}}_p(t) = \frac{\hbar}{m}\nabla\Phi\Big|_{\mathbf{r}=\mathbf{r}_p(t)}. \tag{5}$$

This equation is motivated by the Madelung transformation [30]. The two coupled particle-wave equations (2) and (5) are nonlinear and in general hard to solve. They should be supplemented with the appropriate initial and boundary conditions, e.g., those of standard quantum mechanics. Note that we need to specify the initial condition of the entire wave field together with the position of the particle. The particle velocity will then be given by Eq. (5). This means that the notion of a "particle at position P moving with velocity $\mathbf{v}$" must be supplemented with the specification of the entire background field to allow the prediction of the future particle orbit. If, for some reason, only the particle properties were directly measurable, this would imply an "uncertainty relation" for the particle, even though the system is completely deterministic.

The solution of Eq. (2) may formally be given in terms of the particle trajectory $\mathbf{r}_p(t)$ using the Feynman propagator $K(\mathbf{r},t;\mathbf{r}',t')$ satisfying ([31], p. 81)

$$\left(i\hbar\frac{\partial}{\partial t} - \hat{H}\right)K(\mathbf{r},t;\mathbf{r}',t') = i\hbar\,\delta(\mathbf{r}-\mathbf{r}')\delta(t-t'), \tag{6}$$

where causality requires that $K(\mathbf{r},t;\mathbf{r}',t')$ is only nonzero for $t' < t$. Thus, we assume that the particle can make disturbances only *forward in time*. Rewriting the source term as

$$J(\mathbf{r},t) = \int_{-\infty}^{\infty} A(t')\,\delta[\mathbf{r} - \mathbf{r}_p(t')]\,\delta(t-t')dt', \tag{7}$$

we then get the solution

$$\begin{aligned}\Psi(\mathbf{r},t) &= \frac{1}{i\hbar}\int_{-\infty}^{t} K[\mathbf{r},t;\mathbf{r}_p(t'),t']A(t')dt' \\ &= \frac{1}{i\hbar}\int_{0}^{\infty} K[\mathbf{r},t;\mathbf{r}_p(t-\tau),t-\tau]A(t-\tau)d\tau.\end{aligned} \tag{8}$$

B. Free particle

For a free particle we have

$$\hat{H} = -\frac{\hbar^2}{2m}\nabla^2 \tag{9}$$

and the Feynman propagator in D spatial dimensions is ([31], p. 42)

$$K_f(\mathbf{r},t;\mathbf{r}',t') = \left[\frac{m}{2\pi i\hbar(t-t')}\right]^{D/2}\exp\left[\frac{im|\mathbf{r}-\mathbf{r}'|^2}{2\hbar(t-t')}\right]. \tag{10}$$

Let us now assume that the particle moves on a straight line $\mathbf{r}_p(t) = \mathbf{v}t$, where the velocity $\mathbf{v}$ is constant. Then, the solution of Eq. (2) is, taking for simplicity $A(t) = 1$,

$$\begin{aligned}\Psi(\mathbf{r},t) &= \frac{1}{i\hbar}\int_0^{\infty} K_f[\mathbf{r},t;\mathbf{v}(t-\tau),t-\tau]d\tau \\ &= \frac{1}{i\hbar}\int_0^{\infty}\left(\frac{m}{2\pi i\hbar\tau}\right)^{D/2}\exp\left[\frac{im|\mathbf{r}-\mathbf{v}(t-\tau)|^2}{2\hbar\tau}\right]d\tau\end{aligned} \tag{11}$$

and in three dimensions ($D = 3$) the solution becomes

$$\Psi(\mathbf{r},t) = \frac{m}{2\pi\hbar^2}\frac{1}{|\mathbf{r}-\mathbf{v}t|}e^{i\frac{m}{\hbar}[\mathbf{v}\cdot(\mathbf{r}-\mathbf{v}t)+|\mathbf{v}||\mathbf{r}-\mathbf{v}t|]}. \tag{12}$$

In two dimensions (which is perhaps closer to the experiment), we get

$$\Psi(\mathbf{r},t) = \frac{m}{2i\hbar^2}e^{i\frac{m}{\hbar}[\mathbf{v}\cdot(\mathbf{r}-\mathbf{v}t)]}H_0^{(1)}\left(\frac{m}{\hbar}|\mathbf{v}||\mathbf{r}-\mathbf{v}t|\right), \tag{13}$$

where $H_0^{(1)}(x)$ is the Hankel function of first kind of order zero. The cometlike shape of this wave function is apparent [Fig. 13(a)] and resembles the surface waves created by a walker [25]. The gradient of the phase is, however, discontinuous at the location of the particle since for $D = 3$,

$$\frac{\hbar}{m}\nabla\Phi = \mathbf{v} + |\mathbf{v}|\frac{\mathbf{r}-\mathbf{v}t}{|\mathbf{r}-\mathbf{v}t|}, \tag{14}$$

which is $(\hbar/m)\nabla\Phi = 2\mathbf{v}$ immediately in front of the particle and $\nabla\Phi = 0$ behind it. Averaging over a small spherical shell around the current position of the particle yields the expected $(\hbar/m)\langle\nabla\Phi\rangle = \mathbf{v} = \mathbf{v}_p$.

The discontinuity in the gradient of the phase may be removed by requiring Galilean invariance. Equations (2)–(5) are not in general Galilean invariant. The same goes for the experiment, as pointed out by Fort and Couder [32], since the liquid bath acts like an "ether" selecting a preferred frame of reference. The Schrödinger equation for a free particle *is*, however, Galilean covariant in the sense that the transformation

$$\mathbf{r}' = \mathbf{r} - \mathbf{v}_g t, \tag{15}$$

$$t' = t, \tag{16}$$

$$\mathbf{v}' = \mathbf{v} - \mathbf{v}_g \tag{17}$$

merely alters the wave function by a phase

$$\Psi(\mathbf{r}',t') = e^{i\phi(\mathbf{r},t)}\Psi(\mathbf{r},t), \tag{18}$$

where

$$\phi(\mathbf{r},t) = -\frac{m}{\hbar}\left(\mathbf{v}_g\cdot\mathbf{r} - \frac{1}{2}v_g^2 t\right). \tag{19}$$

If we demand that this should hold also for our particle-wave dynamics in Eqs. (2)–(5), the source term must, as shown in

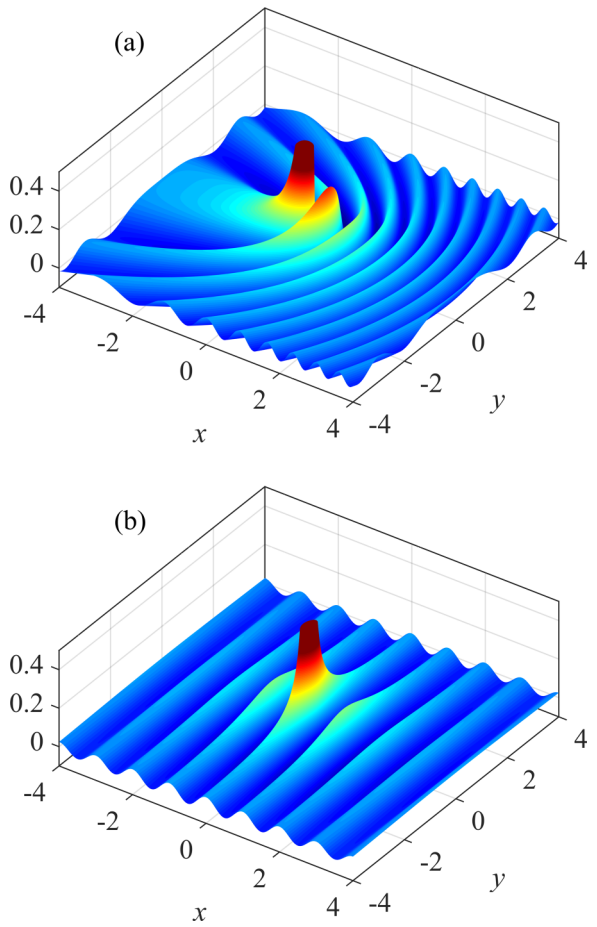

FIG. 13. (Color online) Solutions $\mathrm{Re}(\Psi)$ for a free particle in three dimensions moving on a straight line $\mathbf{r}_p(t) = v\,t\,\hat{\mathbf{x}}$. (a) Non-Galilean invariant case and (b) Galilean invariant case. The x and y coordinates are made dimensionless using the de Broglie wavelength $h/(m\,v)$, we have set $z = 0$ and $t = 0$, and $\mathrm{Re}(\Psi)$ is shown in arbitrary units.

Appendix A, have the form

$$J(\mathbf{r},t) = A_0 e^{i\zeta(t)}\delta[\mathbf{r} - \mathbf{r}_p(t)], \tag{20}$$

where the extra phase for a free particle may be taken to be

$$\zeta(t) = \frac{m}{2\hbar}\int v_p^2(t)dt = \frac{1}{\hbar}\int E_k(t)dt. \tag{21}$$

For a free particle $\zeta(t) = mv^2t/2\hbar$, and instead of the comet-shaped solution presented above, we now get the wave function ($D = 3$, $A_0 = 1$)

$$\Psi_g(\mathbf{r},t) = \frac{1}{i\hbar}\int_{-\infty}^{t} K_f(\mathbf{r},t;\mathbf{v}t',t')\,e^{i\frac{mv^2}{2\hbar}t'}dt'$$
$$= \frac{m}{2\pi\hbar^2}\frac{1}{|\mathbf{r}-\mathbf{v}t|}e^{i\frac{m}{\hbar}(\mathbf{v}\cdot\mathbf{r}-\frac{1}{2}v^2t)}. \tag{22}$$

This plane-wave-like solution [Fig. 13(b)] fulfills Eq. (5) without a discontinuity in the gradient of the phase. The amplitude is, however, both in the Galilean invariant and noninvariant cases infinite at the location of the particle $\mathbf{r} = \mathbf{v}t$, and to study interacting particles we would have to regularize the wave field for instance by introducing a finite size to the particle or representing it by a blinking source in terms of a series of delta functions instead of being continuous in time.

C. Orbital quantization

For a particle moving in a potential $V(\mathbf{r})$, we can choose to generalize Eq. (21) to

$$\zeta(t) = \frac{1}{\hbar}\int E(t)\,dt$$
$$= \frac{m}{2\hbar}\int v_p^2(t)\,dt + \frac{1}{\hbar}\int V[\mathbf{r}_p(t)]\,dt. \tag{23}$$

Note that, in this case, the system is *not* Galilean invariant and neither is the Schrödinger equation.

Let us take as an example the one-dimensional harmonic potential $V(x) = (1/2)\,m\,\omega^2\,x^2$. In this case, we do not know how to solve Eqs. (2)–(5). As an approximation, we assume that the particle executes *classical* motion of the form

$$x_p(t) = R\cos\omega t, \tag{24}$$
$$v_p(t) = -\omega R\sin\omega t, \tag{25}$$

and thus that the total mechanical energy is

$$E = \tfrac{1}{2}mv_p^2 + \tfrac{1}{2}m\omega^2x_p^2 = \tfrac{1}{2}m\omega^2R^2. \tag{26}$$

The source term becomes (with $A_0 = 1$)

$$J(x,t) = \delta[x - x_p(t)]e^{\frac{i}{\hbar}Et}. \tag{27}$$

The propagator for the one-dimensional harmonic oscillator is ([31], p. 200)

$$K(x,t;x',t') = \left\{\frac{m\omega}{2\pi i\hbar\sin[\omega(t-t')]}\right\}^{1/2}$$
$$\times\exp\left(\frac{im\omega}{2\hbar\sin[\omega(t-t')]}\{(x^2+x'^2)\right.$$
$$\left.\times\cos[\omega(t-t')] - 2xx'\}\right), \tag{28}$$

which when inserted into Eq. (8) yields for the wave field

$$\Psi(x,t) = -\frac{1}{i\hbar}\left(\frac{m\omega}{2\pi i\hbar}\right)^{1/2}\int_0^\infty\frac{d\tau}{\sqrt{\sin(\omega\tau)}}\exp\left[\frac{i}{\hbar}E(t-\tau)\right]$$
$$\times\exp\left[\frac{im\omega}{2\hbar}\left(\left\{x^2 + R^2\cos^2[\omega(t-\tau)]\right\}\cot(\omega\tau)\right.\right.$$
$$\left.\left. - 2xR\frac{\cos[\omega(t-\tau)]}{\sin(\omega\tau)}\right)\right]. \tag{29}$$

Except for the phase factor $\exp(-iE\tau/\hbar)$, the integrand is periodic with period $T = 2\pi/\omega$. Denoting the periodic part as $f_T(\tau)$, the integral for Ψ has the form

$$\int_0^\infty f_T(\tau)e^{-i\frac{E\tau}{\hbar}}d\tau = \sum_{k=0}^{\infty}\int_0^T f_T(\tau+kT)e^{-i\frac{E}{\hbar}(\tau+kT)}d\tau$$
$$= \sum_{k=0}^{\infty}e^{-i\frac{EkT}{\hbar}}\int_0^T f_T(\tau)e^{-i\frac{E}{\hbar}\tau}d\tau$$
$$= \frac{1}{1-e^{-i\frac{ET}{\hbar}}}\int_0^T f_T(\tau)e^{-i\frac{E}{\hbar}\tau}d\tau \tag{30}$$

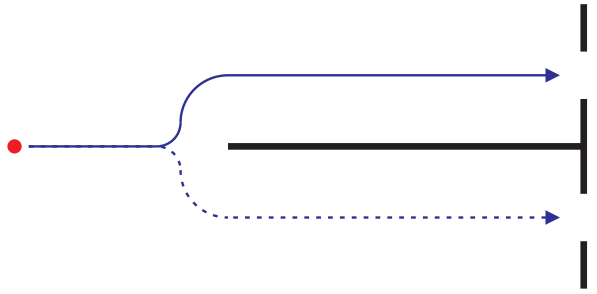

FIG. 14. (Color online) Double-slit experiment with a splitter plate. A particle will have to move on one or the other side of the plate as shown by the two possible trajectories.

and we see that the full integral is resonant for $\exp(-iET/\hbar) = 1$, i.e., for $ET/\hbar = 2\pi n$, where $n = 1,2,\ldots$. This leads us to the energy quantization

$$E = n\hbar\omega, \tag{31}$$

which is identical to the Bohr-Sommerfeld quantization rule [33]. This shows that orbital quantization is indeed possible in our simple model of wave-driven particles.

D. Double-slit experiment

To explore how superposition of states unfold in our model we now return to the modified version of the double-slit experiment with a splitter plate. As discussed earlier, the presence of the splitter plate does not qualitatively alter the quantum mechanical interference pattern (Sec. III). For our model of wave-driven particles, this is not so. The particle reaching the splitter plate will unavoidably have to proceed along one side or the other (Fig. 14). The field at the "chosen" side behaves roughly like our stationary solution for a free particle [Fig. 13(b)] while it moves towards the slit. The field on the "other" side, however, has basically no source term since the source is on the chosen side of the splitter plate, and the wave packet on the other side will therefore slowly disperse. With a sufficiently long splitter plate, the particle emerging from the chosen slit will thus only experience an extremely weak influence from the other slit, which would not be able to deflect it. Correspondingly, the particle statistics would approach the classical result: the superposition of the probability distributions for each single slit without interference.

To solve our particle-wave problem in Eqs. (2)–(5) for a particle impinging on a splitter plate is hard and beyond our present capacity. Roughly, the solution on the chosen side of the splitter plate, where the particle is, will propagate like the free particle solution with unchanged form due to the source term. The fact that the splitter plate is present will create an image, but if the particle is not too close to the plate this will not alter the wave function qualitatively. The wave field on the other side of the splitter plate will propagate according to the standard Schrödinger equation, with no source term, since the source is on the chosen side of the splitter plate. Assuming at time $t = 0$ an initial state such as our Galilean invariant solution (22), the wave function will as shown in

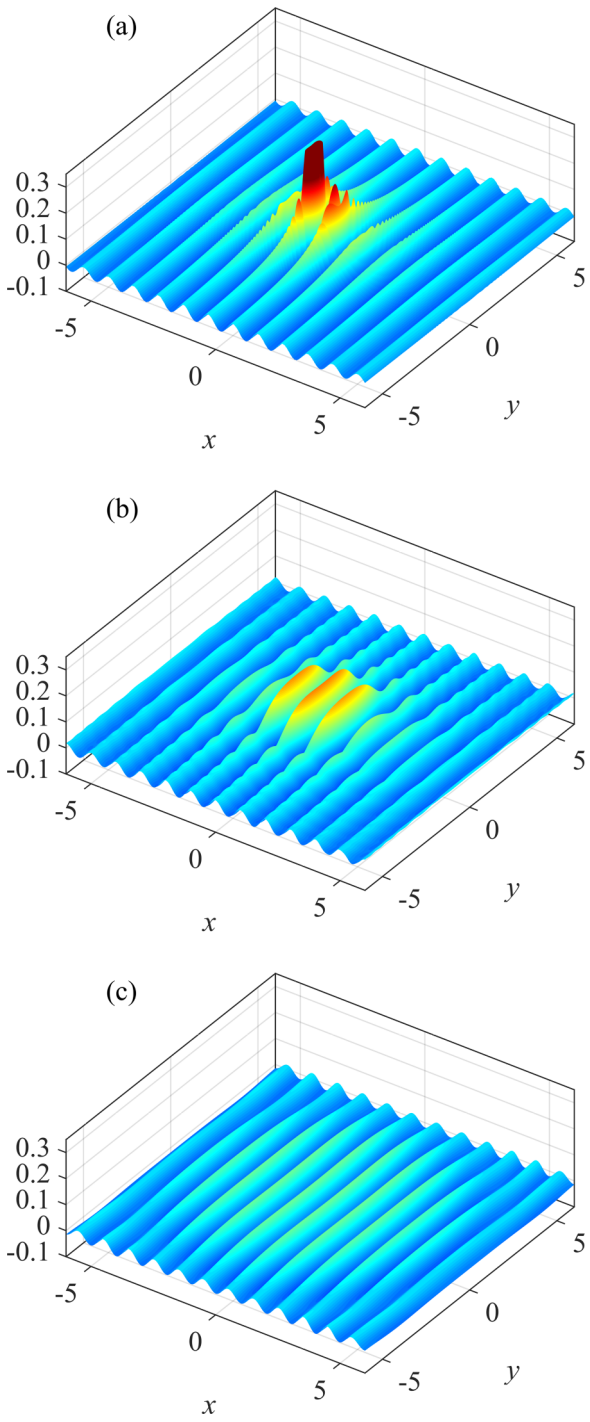

FIG. 15. (Color online) Time evolution of the wave field Re(Ψ) without a particle at times (a) $t = 0.6$, (b) $t = 2$, and (c) $t = 5$. The x and y coordinates are made dimensionless using the de Broglie wavelength $h/(m\,v)$, the time t using the period $2\,h/(m\,v^2)$, we have set $z = 0$, and Re(Ψ) is shown in arbitrary units.

Appendix B at a later time t have the form

$$\Psi(\mathbf{r},t) = \frac{2}{\sqrt{\pi i}}\,\Psi_g(\mathbf{r},t)\,F\left(|\mathbf{r}-\mathbf{v}t|\sqrt{\frac{m}{2\hbar t}}\right), \tag{32}$$

where $F(u) = \int_0^u \exp(it^2)\,dt$, which slowly disperses (Fig. 15). The singularity of Ψ_g at $\mathbf{r} = \mathbf{v}t$ is immediately

eliminated and the wave field slowly decays into a plane wave of amplitude $A \sim 1/\sqrt{t}$ within a circular patch of radius $R \sim \sqrt{t}$. By increasing the length of the splitter plate, and thereby the time $t \sim L/v$ it takes the particle-free wave to reach its slit, we decrease its amplitude, and the position of the center becomes increasingly ill defined. For a sufficiently long splitter plate, the wave field that goes through the other slit would thus cause weak and imprecise wave interference, too feeble to significantly alter the path of the particle, and we would obtain the classical result: a sum of the two single-slit diffraction patterns. Since this is contrary to quantum mechanics, our model fails to reproduce the full range of quantum mechanical phenomena.

V. DISCUSSION AND OUTLOOK

In our double-slit experiment with walking droplets we do not find support for an interference pattern (Sec. II). In fact, the long and variable slit passage times of the droplets, together with the weakness of the wave field through the other slit, cast strong doubt on the feasibility of the interference reported by Couder and Fort [7].

For the more detailed comparison, we emphasize that the placement of the droplet source is most likely very significant when comparing the single-particle statistics in the double-slit experiment with results in the single-slit experiment as reference. Presumably, the single-particle statistics would be altered, e.g., if the droplet source in the double-slit experiment was moved and directed towards the midpoint of one of the slits or if a subset of the trajectories with particular impact parameters was singled out. How to choose between a well-defined point source and a plane wave source and experimentally realize the most clean comparison between the double-slit experiment and a reference experiment to test only the effect of the second slit therefore remains, in our opinion, an open question.

The second slit in the double-slit experiment results in a change of the boundary condition for the wave field behind the slit arrangement. This change of boundary condition could possibly affect the single-particle statistics in a way that is unrelated to interference between wave field components following different paths through the double-slit arrangement. Furthermore, in our experimental realization it appears that the wave field through the other slit in the double-slit experiment is weak, and we believe that this might be a common feature in other experimental realizations in which the width of the slit is smaller or comparable to the Faraday wavelength. Finally, the strength of the wave field passing through the other slit could probably be increased by working closer to the Faraday threshold. This, however, conflicts with the notion of a localized wave field around the droplet as the wave field starts to reach out to the boundaries of the finite container. The chosen forcing amplitude therefore represents a compromise. We are currently working to measure wave field heights in the single-slit and double-slit experiments to explore the possible interference mechanism quantitatively.

In our analysis, we argued that the double-slit experiment with a splitter plate would behave very differently for wave-driven particles and standard quantum mechanics since the interference between the particle and the wave it generates through the other slit would be gradually lost when the length of the splitter plate increases (Sec. IV). In the quantum case, the interference pattern would of course also be gradually lost, but only because the intensity of the signal going through the two slits would become very weak due to spreading and diffraction of the wave packet (Sec. III). However, in the absence of external noise, the parts of the wave going through the two slits would still be in phase due to the symmetry of the slit arrangement and hence the interference pattern would, for any finite splitter plate length, be detectable with sufficiently sensitive measuring devices and sufficiently long measuring times.

This would not be true for the wave-driven particles. For a long splitter plate, the two signals coming out of each of the two slits will be very different: one will be a "particle" and the other will be weak debris from a particle, i.e., the remnants of the wave packet remaining on the side of the splitter plate that the particle did not choose. It is of course true that the probability for a particle to get through the slits would change due to the existence of the splitter plate, which again would mean that long measuring times might be required, but the particles that do get through will, in the case of a long splitter plate, only be exposed to a very weak interference from the other slit and thus only experience very slight deviations from their course.

Thus, there is a qualitative difference between quantum mechanics and our particle-wave dynamics that stems from the fact that phase coherence cannot be maintained in the particle-wave dynamics since the path selected by the particle contributes in a fundamentally different way than other possible paths. How this asymmetry develops depends of course on the exact form of the particle-wave theory. However, the above arguments are general, relying only on the dispersive nature of the waves, which seems unavoidable since particles with different wavelengths should travel with different speeds. This implies generally that an initially localized disturbance will, when propagated by the unforced equation, spread out and decay and thus behave very differently from the forced case, where a particle can move forever without a change of wave shape.

ACKNOWLEDGMENTS

We are thankful to M. Bjørn, J. Bush, Y. Couder, A. Eddi, E. Fort, D. Harris, and M. Nielsen for many stimulating discussions, and we thank E. Hansen for his careful work in designing and constructing the experimental setup.

APPENDIX A: GALILEAN INVARIANCE OF SOURCE TERM

To obtain the Galilean invariant form of the source term in Eq. (2) for a free particle, i.e., Eqs. (20) and (21), we demand that the Galilean transformation

$$\mathbf{r}' = \mathbf{r} - \mathbf{v}_g t, \tag{A1}$$

$$t' = t, \tag{A2}$$

$$\mathbf{v}' = \mathbf{v} - \mathbf{v}_g \tag{A3}$$

merely alters the solution Ψ of the wave-particle equation for a free particle

$$\Psi(\mathbf{r},t) = \frac{1}{i\hbar}\int_0^\infty K_f[\mathbf{r},t;\mathbf{r}_p(t-\tau),t-\tau]A(t-\tau)d\tau \quad \text{(A4)}$$

by a phase as

$$\Psi(\mathbf{r}',t') = e^{i\phi(\mathbf{r},t)}\Psi(\mathbf{r},t). \quad \text{(A5)}$$

Note that in this appendix, a prime does *not* denote a derivative, but a transformed variable. We now assume that the source strength $A(t)$ includes a time dependent phase factor, i.e.,

$$A(t) = A_0 e^{i\zeta(t)}, \quad \text{(A6)}$$

where we shall take $A_0 = 1$ for simplicity. In the transformed system, we then get

$$\Psi'(\mathbf{r}',t) = \frac{1}{i\hbar}\int_0^\infty K_f[\mathbf{r}',t;\mathbf{r}'_p(t-\tau),t-\tau]e^{i\zeta'(t-\tau)}d\tau, \quad \text{(A7)}$$

where we have used that $t' = t$, and where K_f is given by Eq. (10), which can be written in the form

$$K_f[\mathbf{r}',t;\mathbf{r}'_p(t-\tau),t-\tau] = \left(\frac{m}{2\pi i\hbar\tau}\right)^{D/2} e^{\frac{im}{2\hbar}z'(t,\tau)}, \quad \text{(A8)}$$

where

$$z(t,\tau) = \frac{|\mathbf{r}-\mathbf{r}_p(t-\tau)|^2}{\tau}, \quad \text{(A9)}$$

so that

$$\begin{aligned} z'(t,\tau) &= \frac{|\mathbf{r}'-\mathbf{r}'_p(t-\tau)|^2}{\tau} = \frac{|\mathbf{r}-\mathbf{r}_p(t-\tau)-\mathbf{v}_g\tau|^2}{\tau} \\ &= z(t,\tau) - 2\mathbf{v}_g\cdot[\mathbf{r}-\mathbf{r}_p(t-\tau)] + v_g^2\tau \\ &= z(t,\tau) + \frac{2\hbar}{m}\phi(\mathbf{r},t) - \frac{2\hbar}{m}\phi[\mathbf{r}_p(t-\tau),t-\tau], \end{aligned} \quad \text{(A10)}$$

where

$$\phi(\mathbf{r},t) = -\frac{m}{\hbar}\left(\mathbf{v}_g\cdot\mathbf{r} - \frac{1}{2}v_g^2 t\right) \quad \text{(A11)}$$

as in quantum mechanics for a free particle [34]. Thus,

$$K_f[\mathbf{r}',t;\mathbf{r}'_p(\bar{t}),\bar{t}] = K_f[\mathbf{r},t;\mathbf{r}_p(\bar{t}),\bar{t}]e^{i\{\phi(\mathbf{r},t)-\phi[\mathbf{r}_p(\bar{t}),\bar{t}]\}} \quad \text{(A12)}$$

and, from Eq. (A7) we find

$$\zeta'(t) - \zeta(t) = \phi[\mathbf{r}_p(t),t]. \quad \text{(A13)}$$

By taking the total derivative with respect to time of Eq. (A13) we find for the phase $\zeta(t)$, with $\mathbf{v}'_p = \mathbf{v}_p - \mathbf{v}_g$,

$$\begin{aligned} \frac{d}{dt}[\zeta'(t)-\zeta(t)] &= \frac{d}{dt}\phi[\mathbf{r}_p(t),t] \\ &= \frac{\partial\phi}{\partial t} + \mathbf{v}_p\cdot\nabla\phi \\ &= \frac{mv_g^2}{2\hbar} - \frac{m}{\hbar}\mathbf{v}_g\cdot\mathbf{v}_p \\ &= \frac{mv_p'^2}{2\hbar} - \frac{mv_p^2}{2\hbar} \end{aligned} \quad \text{(A14)}$$

so that we can take

$$\zeta(t) = \frac{m}{2\hbar}\int v_p^2(t)dt = \frac{1}{\hbar}\int E_k(t)dt \quad \text{(A15)}$$

in accordance with Eq. (21). In addition, it is obvious from Eq. (A11) that the "guidance" equation (5) is Galilean invariant as well.

APPENDIX B: PROPAGATION WITHOUT A SOURCE TERM

To obtain the solution in Eq. (32), we consider the situation when there is no source term J in Eq. (2) and an initial state is propagated forwards in time by standard quantum mechanics. This is assumed to happen, e.g., for the wave field created on the side of the splitter plate where there is no particle.

The Galilean invariant solution for a free particle moving on a straight line $\mathbf{r} = \mathbf{v}t$ in $D = 3$ is given in Eq. (22) as

$$\Psi_g(\mathbf{r},t) = \frac{A}{|\mathbf{r}-\mathbf{v}t|}e^{ia(2\mathbf{v}\cdot\mathbf{r}t - v^2t^2)}, \quad \text{(B1)}$$

where $A = m/(2\pi\hbar^2)$ and $a = m/(2\hbar t)$. If we take this as the initial state at $t = 0$ and assume no source term, we find for a later time

$$\begin{aligned} \Psi(\mathbf{r},t) &= \int d^3r' K_f(\mathbf{r},t;\mathbf{r}',0)\Psi_g(\mathbf{r}',0) \\ &= A\left(\frac{a}{\pi i}\right)^{3/2}\int d^3r'\frac{1}{r'}e^{ia(|\mathbf{r}-\mathbf{r}'|^2+2\mathbf{r}'\cdot\mathbf{v}t)} \\ &= A\left(\frac{a}{\pi i}\right)^{3/2}e^{iar^2}\int d^3r'\frac{1}{r'}e^{ia(r'^2-2\mathbf{b}\cdot\mathbf{r}')}, \end{aligned} \quad \text{(B2)}$$

where $\mathbf{b} = \mathbf{r} - \mathbf{v}t$ and K_f is given by Eq. (10). Now,

$$\begin{aligned} &\int d^3r'\frac{1}{r'}e^{ia(r'^2-2\mathbf{b}\cdot\mathbf{r}')} \\ &= 2\pi\int_0^\infty ds\, e^{ias^2}s\int_{-1}^1 dx\, e^{-2iabsx} \\ &= 2\pi\int_0^\infty ds\, e^{ias^2}s\left(\frac{1}{2iabs}\right)(e^{2iabs} - e^{-2iabs}) \\ &= \frac{\pi}{iab}\int_0^\infty [e^{i(as^2+2abs)} - e^{i(as^2-2abs)}]ds \\ &= \frac{\pi}{iab}e^{-iab^2}\int_0^\infty [e^{ia(s+b)^2} - e^{ia(s-b)^2}]ds \\ &= \frac{\pi}{ia^{3/2}b}e^{-iab^2}\left[\int_{-b\sqrt{a}}^\infty e^{it^2}\,dt - \int_{b\sqrt{a}}^\infty e^{it^2}\,dt\right] \\ &= \frac{2\pi}{ia^{3/2}b}e^{-iab^2}[C(b\sqrt{a}) + i\,S(b\sqrt{a})] \\ &= \frac{2\pi}{ia^{3/2}b}e^{-iab^2}F(b\sqrt{a}), \end{aligned} \quad \text{(B3)}$$

where we have chosen the polar axis along $\mathbf{r} - \mathbf{v}t$ and $x = \cos\theta$. Further C, S, and F are the integrals:

$$C(u) = \int_0^u \cos(t^2)\,dt, \quad \text{(B4)}$$

$$S(u) = \int_0^u \sin(t^2)\,dt, \tag{B5}$$

$$F(u) = \int_0^u e^{it^2}\,dt. \tag{B6}$$

Inserting the result in Eq. (B3) into Eq. (B2), we get

$$\begin{aligned}\Psi(\mathbf{r},t) &= A\left(\frac{a}{\pi i}\right)^{3/2} e^{iar^2}\frac{2\pi}{ia^{3/2}b}e^{-iab^2}[\mathrm{C}(b\sqrt{a}) + i\mathrm{S}(b\sqrt{a})] \\ &= \frac{2A}{\sqrt{\pi i}}e^{i\frac{m}{2\hbar}(2\mathbf{r}\cdot\mathbf{v}-v^2t)}\frac{1}{|\mathbf{r}-\mathbf{v}t|}F\left(|\mathbf{r}-\mathbf{v}t|\sqrt{\frac{m}{2\hbar t}}\right) \\ &= \frac{2}{\sqrt{\pi i}}\Psi_g(\mathbf{r},t)\,F\left(|\mathbf{r}-\mathbf{v}t|\sqrt{\frac{m}{2\hbar t}}\right).\end{aligned} \tag{B7}$$

Note that $F(u) \to (1/2)(\pi i)^{1/2}$ for $u \to \infty$, so $\Psi(\mathbf{r},t) \to \Psi_g(\mathbf{r},t)$ for $t \to 0$ as it should. Contrary to Ψ_g, $\Psi(\mathbf{r},t)$ does not diverge at $\mathbf{r} = \mathbf{v}t$ since $u^{-1}C(u) \to 1$ and $u^{-1}S(u) \to 0$ for $u \to 0$. For $|\mathbf{r}-\mathbf{v}t| \ll \sqrt{2\hbar t/m}$ the wave field has the form

$$\Psi(\mathbf{r},t) \approx \frac{2A}{\sqrt{\pi i}}e^{i\frac{m}{2\hbar}(2\mathbf{r}\cdot\mathbf{v}-v^2t)}\sqrt{\frac{m}{2\hbar t}}, \tag{B8}$$

i.e., a plane wave with amplitude decreasing as $1/\sqrt{t}$. For $|\mathbf{r}-\mathbf{v}t| \gg \sqrt{2\hbar t/m}$ the amplitude of $\Psi(\mathbf{r},t)$ becomes very small, so the radius of the spherical plane wave region grows as $\sqrt{t}$ (Fig. 15).

[1] T. B. Benjamin and F. Ursell, Proc. R. Soc. London A **225**, 505 (1954).
[2] K. Kumar and L. S. Tuckerman, J. Fluid Mech. **279**, 49 (1994).
[3] Y. Couder, E. Fort, C.-H. Gautier, and A. Boudaoud, Phys. Rev. Lett. **94**, 177801 (2005).
[4] Y. Couder, S. Protière, E. Fort, and A. Boudaoud, Nature (London) **437**, 208 (2005).
[5] S. Protière, Y. Couder, E. Fort, and A. Boudaoud, J. Phys.: Condens. Matter **17**, S3529 (2005).
[6] S. Protière, A. Boudaoud, and Y. Couder, J. Fluid Mech. **554**, 85 (2006).
[7] Y. Couder and E. Fort, Phys. Rev. Lett. **97**, 154101 (2006).
[8] E. Fort, A. Eddi, A. Boudaoud, J. Moukhtar, and Y. Couder, Proc. Natl. Acad. Sci. USA **107**, 17515 (2010).
[9] A. Eddi, J. Moukhtar, S. Perrard, E. Fort, and Y. Couder, Phys. Rev. Lett. **108**, 264503 (2012).
[10] D. M. Harris and J. W. M. Bush, J. Fluid Mech. **739**, 444 (2014).
[11] A. U. Oza, D. M. Harris, R. R. Rosales, and J. W. M. Bush, J. Fluid Mech. **744**, 404 (2014).
[12] S. Perrard, M. Labousse, M. Miskin, E. Fort, and Y. Couder, Nat. Commun. **5**, 3219 (2014).
[13] S. Perrard, M. Labousse, E. Fort, and Y. Couder, Phys. Rev. Lett. **113**, 104101 (2014).
[14] A. Eddi, E. Fort, F. Moisy, and Y. Couder, Phys. Rev. Lett. **102**, 240401 (2009).
[15] D. M. Harris, J. Moukhtar, E. Fort, Y. Couder, and J. W. M. Bush, Phys. Rev. E **88**, 011001(R) (2013).
[16] J. Moláček and J. W. M. Bush, J. Fluid Mech. **727**, 582 (2013).
[17] J. Moláček and J. W. M. Bush, J. Fluid Mech. **727**, 612 (2013).
[18] A. U. Oza, R. R. Rosales, and J. W. M. Bush, J. Fluid Mech. **737**, 552 (2013).
[19] Ø. Wind-Willassen, J. Moláček, D. M. Harris, and J. W. M. Bush, Phys. Fluids **25**, 082002 (2013).
[20] J. W. M. Bush, Annu. Rev. Fluid Mech. **47**, 269 (2015).
[21] L. de Broglie, Ann. Fond. Louis de Broglie **12**, 1 (1987).
[22] J. W. M. Bush, Proc. Natl. Acad. Sci. USA **107**, 17455 (2010).
[23] Y. Couder and E. Fort, J. Phys.: Conf. Ser. **361**, 012001 (2012).
[24] D. M. Harris and J. W. M. Bush, J. Sound Vibrat. **334**, 255 (2015).
[25] A. Eddi, E. Sultan, J. Moukhtar, E. Fort, M. Rossi, and Y. Couder, J. Fluid Mech. **674**, 433 (2011).
[26] W. H. Press, S. A. Teukolsky, W. T. Vetterling, and B. P. Flannery, *Numerical Recipes*, 3rd ed. (Cambridge University Press, Cambridge, UK, 2007).
[27] D. Bohm, Phys. Rev. **85**, 166 (1952).
[28] D. Bohm, Phys. Rev. **85**, 180 (1952).
[29] D. Bohm, Phys. Rev. **89**, 458 (1953).
[30] E. Madelung, Z. Phys. **40**, 322 (1927).
[31] R. P. Feynman and A. R. Hibbs, *Quantum Mechanics and Path Integrals* (Dover, New York, 2010).
[32] E. Fort and Y. Couder, Europhys. Lett. **102**, 16005 (2013).
[33] N. Bohr, D. Kgl. Danske Vidensk. Selsk. Skrifter, Naturvidensk. og Mathem. Afd. 8. Række, IV.1, 1–3 (1918).
[34] E. Merzbacher, *Quantum Mechanics*, 3rd ed. (Wiley, New York, 1998).